Non-Hermitian dynamics and $\mathcal{PT}$-symmetry breaking in interacting mesoscopic Rydberg platforms

José A. S. Lourenço,[1,2] Gerard Higgins,[2] Chi Zhang,[2] Markus Hennrich,[2] and Tommaso Macrì[1]
[1]*Departamento de Física Teórica e Experimental, Universidade Federal do Rio Grande do Norte, Campus Universitário, Lagoa Nova, Natal, Rio Grande do Norte, 59072-970, Brazil*
[2]*Department of Physics, Stockholm University, 10691 Stockholm, Sweden*

(Received 11 November 2021; revised 5 July 2022; accepted 1 August 2022; published 11 August 2022)

We simulate the dissipative dynamics of a mesoscopic system of long-range interacting particles which can be mapped into non-Hermitian spin models with a $\mathcal{PT}$ symmetry. We find rich $\mathcal{PT}$ phase diagrams with $\mathcal{PT}$-symmetric and $\mathcal{PT}$-broken phases. The dynamical regimes can be further enriched by modulating tunable parameters of the system. We outline how the $\mathcal{PT}$ symmetries of such systems may be probed by studying their dynamics. We note that systems of Rydberg atoms and systems of Rydberg ions with strong dipolar interactions are particularly well suited for such studies. We present a viable proposal for implementing non-Hermitian physics with $\mathcal{PT}$ symmetry in Rydberg systems. We show that for realistic parameters, long-range interactions allow the emergence of new $\mathcal{PT}$-symmetric regions, generating new $\mathcal{PT}$ phase transitions. In addition, such $\mathcal{PT}$-symmetry phase transitions are found by changing the configurations of the Rydberg atoms. We propose a postselection scheme on an ensemble of Rydberg ions described by an effective three-level system. Detecting the population dynamics, the system shows an oscillatory behavior in the $\mathcal{PT}$-unbroken phase and a stationary population for long times in the $\mathcal{PT}$-broken phase.

DOI: 10.1103/PhysRevA.106.023309

I. INTRODUCTION

Closed quantum systems evolve with unitary dynamics according to the Schrödinger equation; the Hamiltonian of such a system is Hermitian and the eigenenergies are real. A dissipative quantum system evolves with nonunitary dynamics, which, in some cases, can be approximately described according to a non-Hermitian Hamiltonian [1–3]. Some of these systems are invariant under the simultaneous application of parity ($\mathcal{P}$) and time-reversal ($\mathcal{T}$) symmetry operators [4]. If all the eigenenergies of the non-Hermitian Hamiltonian are real, a system is said to preserve $\mathcal{PT}$ symmetry, otherwise if part of the spectrum is complex, $\mathcal{PT}$ symmetry will be broken [5]. The critical values that limit the $\mathcal{PT}$-unbroken and $\mathcal{PT}$-broken phases are the exceptional points [6,7]. Also, the existence of a continuous set of exceptional points that limit regions with $\mathcal{PT}$-unbroken and $\mathcal{PT}$-broken phases are called exceptional lines [8–10]. The $\mathcal{PT}$ symmetry of several dissipative quantum systems has been studied in different contexts, e.g., in optics [11–16], in photonics [17–20], in quantum many-body systems [7,21–40], in systems with topological models [41–51], and in curved space [52]. The $\mathcal{PT}$ transition was verified experimentally for a cold-atomic dissipative Floquet system, in which the $\mathcal{PT}$-symmetry transitions can occur by tuning either the dissipation strength or the coupling strength [53]. Recently, models with Floquet $\mathcal{PT}$-symmetric modulation showed a $\mathcal{PT}$-symmetry transition in square-wave modulation [54,55] and were experimentally demonstrated in a system of noninteracting cold fermions [53]. Experimentally, a single trapped ion was used to investigate the dynamics of $\mathcal{PT}$-symmetric non-Hermitian systems [56,57].

In this work we investigate the non-Hermitian dynamics of a mesoscopic system of few particles coupled via long-range interactions among them [58]. We find that the interactions and geometric arrangement of coupled spins enrich the $\mathcal{PT}$ phase diagrams (Sec. II). The $\mathcal{PT}$ phase can be determined by probing the system's dynamics, and reconstructing the system's eigenenergies (Sec. II A). We also find that by modulating system parameters the $\mathcal{PT}$ nonequilibrium dynamical phase diagrams can be further enriched (Sec. II B). Our analysis is inspired by recent experiments with ultracold Rydberg atoms and ions, which are well suited for experimentally probing these effects. We show that Rydberg platforms are promising for the investigation of $\mathcal{PT}$-symmetric non-Hermitian systems (Sec. III). Furthermore, our model can be generalized to more complete Rydberg atom models and more complex systems [59–70] and can also be implemented on other experimental platforms [71,72].

II. MODEL

We consider a system of N particles each with two internal levels and loss channels to a third auxiliary state. Particles interact via long-range exchange interactions. We are motivated by recent works with strongly interacting Rydberg ions [73], and our model was designed to match this system. In Sec. III we describe in more detail about how this model can be experimentally implemented using Rydberg ions.

The two levels of each particle are labeled by $|1\rangle$ and $|2\rangle$. A third level, $|0\rangle$, represents all the states to which $|1\rangle$ and $|2\rangle$ can decay, with decay rates Γ_1 and Γ_2, respectively. States $|1\rangle$ and $|2\rangle$ are coupled with the coupling strength Ω, as shown

 ©2022 American Physical Society

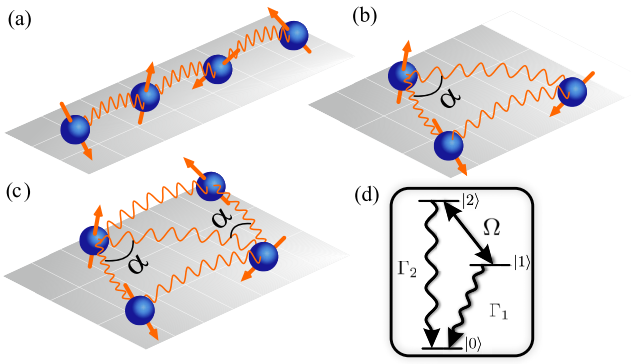

FIG. 1. (a) Linear configuration of interacting four-particles. Zigzag configurations parametrized by angle α: (b) three-particle zigzag and (c) four-particle zigzag. (d) Level scheme of the internal structure of the particles leading to an effective non-Hermitian dynamics. Each particle has two levels, $|1\rangle$ and $|2\rangle$, which are coupled with strength Ω and which decay to a third state $|0\rangle$ with rates Γ_1 and Γ_2, respectively.

in Fig. 1. The ith and jth particles interact with the strength V_{ij}, which can be assumed to be a, e.g., dipolar ($\propto |i-j|^{-3}$) interaction. When written in terms of spin operators, the interaction takes the form of an XY exchange interaction between particles i and j.

The system is described by the density operator $\hat{\rho}(t)$ which evolves according to the master equation

$$\frac{d\hat{\rho}(t)}{dt} = \frac{1}{i\hbar}(\hat{\mathcal{H}}_{\rm eff}\hat{\rho}(t) - \hat{\rho}(t)\hat{\mathcal{H}}_{\rm eff}^{\dagger}) + \Gamma_1 \sum_{n=1}^{N} C_1^n \hat{\rho}(t) C_1^{n\dagger} + \Gamma_2 \sum_{n=1}^{N} C_2^n \hat{\rho}(t) C_2^{n\dagger}, \quad (1)$$

where $C_1 \equiv |0\rangle\langle 1|$ and $C_2 \equiv |0\rangle\langle 2|$ are the collapse operators of the states $|1\rangle$ and $|2\rangle$ to the auxiliary state $|0\rangle$.

The effective non-Hermitian Hamiltonian $\hat{H}_{\rm eff}$ reads

$$\hat{H}_{\rm eff} = \sum_{i=1}^{N} \frac{1}{2}\left[\Omega\hat{\sigma}_x^i - i\Gamma\hat{\sigma}_z^i - i\frac{\Gamma_1+\Gamma_2}{2}\hat{\mathbb{I}}^i\right] + \sum_{i>j}^{N} \frac{V_{ij}}{2}\left(\hat{\sigma}_x^i\hat{\sigma}_x^j + \hat{\sigma}_y^i\hat{\sigma}_y^j\right), \quad (2)$$

where $\hat{\mathbb{I}} = |1\rangle\langle 1| + |2\rangle\langle 2|$ is the identity operator and $\Gamma \equiv (\Gamma_1 - \Gamma_2)/2$. The operators are $\sigma_z = |1\rangle\langle 1| - |2\rangle\langle 2|$, $\hat{\sigma}_x = \hat{\sigma}_+ + \hat{\sigma}_-$, and $\hat{\sigma}_y = -i(\hat{\sigma}_+ - \hat{\sigma}_-)$, and the raising and lowering operators are $\hat{\sigma}_+ = |2\rangle\langle 1|$ and $\hat{\sigma}_- = |1\rangle\langle 2|$, respectively.

We focus on the evolution in the $\{|1\rangle, |2\rangle\}$ manifold, which results in normalized populations $\rho_{1,2}^i$ for each one of the particles. This can be achieved by employing a postselection scheme; experimental sequences conclude with a projective measurement of the populations of the levels of each ion. Only experiments in which the ion remains in the $\{|1\rangle, |2\rangle\}$ manifold are included in the analysis [74]. This approach is a generalization to a mesoscopic number of qubits of a state tomography in a single dissipative transmon qubit realized in Refs. [75,76]. Clearly, increasing the number of ions makes postselection extremely inefficient, at least for long times, due to the exponentially decaying probability that the system populates the $\{|1\rangle, |2\rangle\}$ manifold for each ion.

We notice that, for the case of a single ion, it is possible to derive the populations $\rho_{1,2}(t)$ of the upper state manifold from the population of the auxiliary $|0\rangle$ state. See Appendix A for the detailed calculation.

Importantly, upon subtracting the identity $\hat{\mathbb{I}}$ we obtain a non-Hermitian $\mathcal{PT}$-symmetric Hamiltonian:

$$\hat{\mathcal{H}}_{\mathcal{PT}} = \sum_{i=1}^{N} \frac{1}{2}\left(\Omega\hat{\sigma}_x^i - i\Gamma\hat{\sigma}_z^i\right) + \sum_{i>j}^{N} \frac{V_{ij}}{2}\left(\hat{\sigma}_x^i\hat{\sigma}_x^j + \hat{\sigma}_y^i\hat{\sigma}_y^j\right). \quad (3)$$

Using the parity operator, $\mathcal{P} = \hat{\sigma}_x$, and the time-reversal operator, $\mathcal{T} = K$, where K is the complex conjugate operator, one can show that $\hat{H}_{\mathcal{PT}}$ in Eq. (3) is $\mathcal{PT}$ symmetric, i.e., $(\mathcal{PT})\hat{H}_{\mathcal{PT}}(\mathcal{PT})^{-1} = \hat{H}_{\mathcal{PT}}$. Throughout this work we determine whether $\mathcal{PT}$ is preserved or broken from the eigenvalues of $\hat{H}_{\mathcal{PT}}$: When $\hat{H}_{\mathcal{PT}}$ has real eigenvalues the $\mathcal{PT}$ symmetry is preserved, otherwise the $\mathcal{PT}$ symmetry is broken. Whether the $\mathcal{PT}$ symmetry is preserved or broken depends on the relative strengths of the dissipative part of the Hamiltonian (Γ) and the nondissipative part of the Hamiltonian (Ω and the interactions V_{ij}).

In the following sections we consider the $\mathcal{PT}$-symmetry phase diagrams of different configurations of interacting particles and when the system parameters are modulated.

A. Different configurations of interacting particles

1. Single particle

For a single-particle system ($N = 1$), the eigenvalues of $\hat{H}_{\mathcal{PT}}$ are $\lambda_{\pm} = \pm\Gamma/2\sqrt{(\Omega/\Gamma)^2 - 1}$. The $\mathcal{PT}$ symmetry is preserved when $\Omega/\Gamma > 1$ and the eigenvalues are real. The $\mathcal{PT}$ symmetry is broken when $\Omega/\Gamma < 1$ and the eigenvalues are imaginary. The exceptional point occurs at $\Omega/\Gamma = 1$ and the eigenvalues coalesce and $\lambda_{\pm} = 0$. A system of noninteracting single particles was experimentally studied using ultracold atoms in Ref. [53] and for a single ion in Refs. [56,57].

In the rest of this work, we calculate the eigenvalues of $\hat{H}_{\mathcal{PT}}$ (and thus its $\mathcal{PT}$ symmetry) numerically for different experimentally relevant configurations with realistic interactions.

2. Linear chain of particles

Next we consider a equidistant linear chain of particles, in which the interaction strength falls with the cube of the separation $V_{ij} = V/|i-j|^3$, such as a dipolar interaction. We numerically calculated the eigenvalues of $\hat{H}_{\mathcal{PT}}$ for systems with two, three, and four particles and found the $\mathcal{PT}$ symmetry of $\hat{H}_{\mathcal{PT}}$ depends on the relative strengths of Ω, Γ, and V, as shown in Figs. 2(a)–2(c).

The $\mathcal{PT}$-symmetry phase diagrams become richer with increasing N. While the $N = 2$ case shows a single $\mathcal{PT}$-symmetry-preserving region, more regions are present in the $N = 3$ and $N = 4$ cases. $\mathcal{PT}$ symmetry is preserved when all eigenvalues are real (orange regions), otherwise it is broken (other regions). $\mathcal{PT}$ phase transitions occur along exceptional

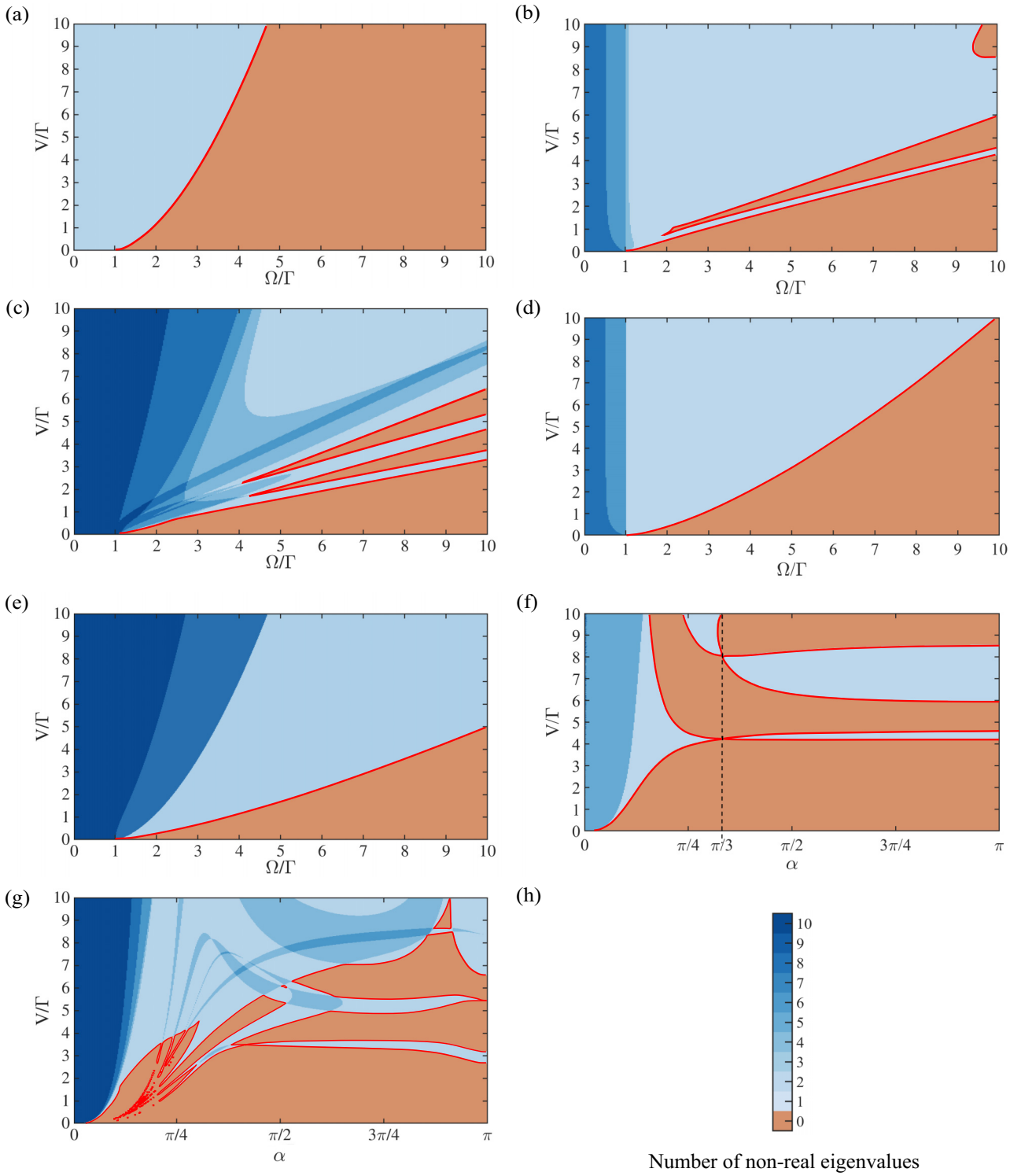

FIG. 2. $\mathcal{PT}$-symmetry phase diagrams for interacting particle systems. The symmetry of $\mathcal{PT}$ is preserved when all eigenvalues are real (orange regions), otherwise it is broken (shaded blue regions). $\mathcal{PT}$-phase transitions occur along exceptional lines (red lines). Panels (a), (b), and (c) show results for $N = 2$, 3, and 4 particles in the linear configuration; the diagrams get richer to increase the number of particles. Panels (d) and (e) show results for particles in a triangular and tetrahedral configuration, respectively. Panels (f) and (g) show results for $N = 3$ and $N = 4$ particles in zigzag configurations. In panel (f) the zigzag configuration becomes an equilateral triangle at $\alpha = \pi/3$, and the symmetry of the system is increased. In panels (f) and (g) we set $\Omega = 10\Gamma$. (h) Color bar with the number of nonreal eigenvalues.

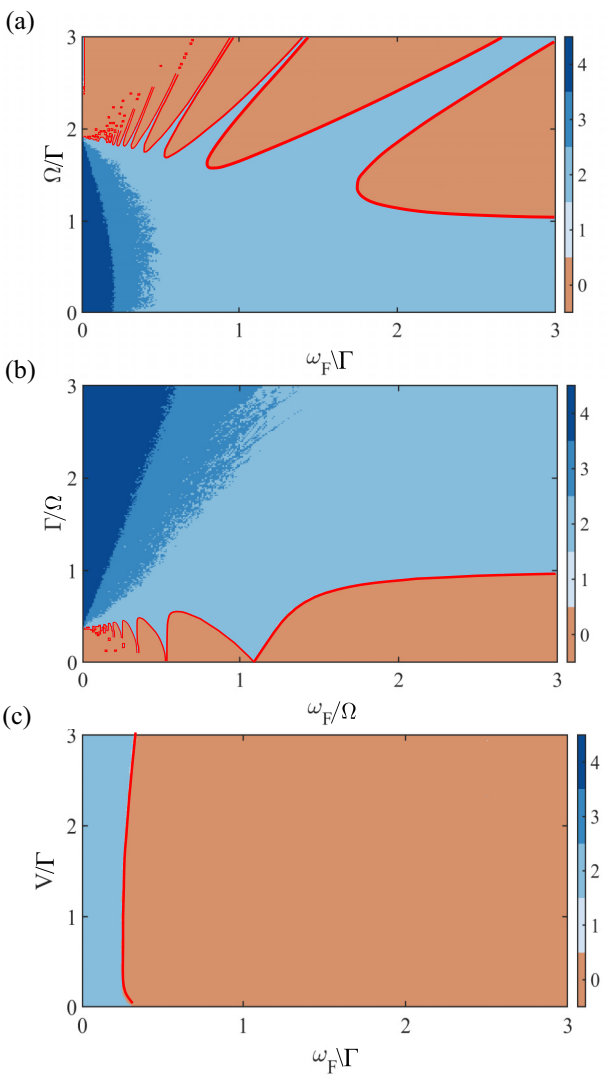

FIG. 3. $\mathcal{PT}$ phase diagrams for two-particle systems when $V(t)$ is sinusoidally modulated at frequency ω_F. $\mathcal{PT}$ symmetry is preserved when all the eigenvalues of the time-evolution operator have unit modulus (orange regions). (a) $\Omega \times \omega_F$ with $V = \Gamma$. (b) $\Gamma \times \omega_F$ with $V = \Omega$. (c) $V \times \omega_F$ with $\Omega = 10\Gamma$. Red lines denote exceptional lines.

lines (red lines) Note that when $V = 0$, the exceptional point at $\Omega/\Gamma = 1$ (for the single-atom case) is recovered.

Figure 4 displays the dynamics of the populations in the $\mathcal{PT}$-symmetric and $\mathcal{PT}$-broken phases after postselection. In Fig. 4(a) we observe an oscillatory behavior of populations of H_{eff} for the region that is $\mathcal{PT}$ symmetric. In Fig. 4(b) the region that is $\mathcal{PT}$ broken is shown. Here the population of state $|1\rangle$ decays and state $|2\rangle$ increases. For longer times the populations saturate to a fixed value.

3. *Equilateral triangular and tetrahedral configurations*

Next we consider three particles arranged in an equilateral triangle configuration and four particles arranged in a tetrahedral configuration. We have $V_{ij} = V$ for each of the particle pairs. We determine whether or not $\hat{H}_{\mathcal{PT}}$ is $\mathcal{PT}$-symmetry preserving by numerically calculating its eigenvalues as the

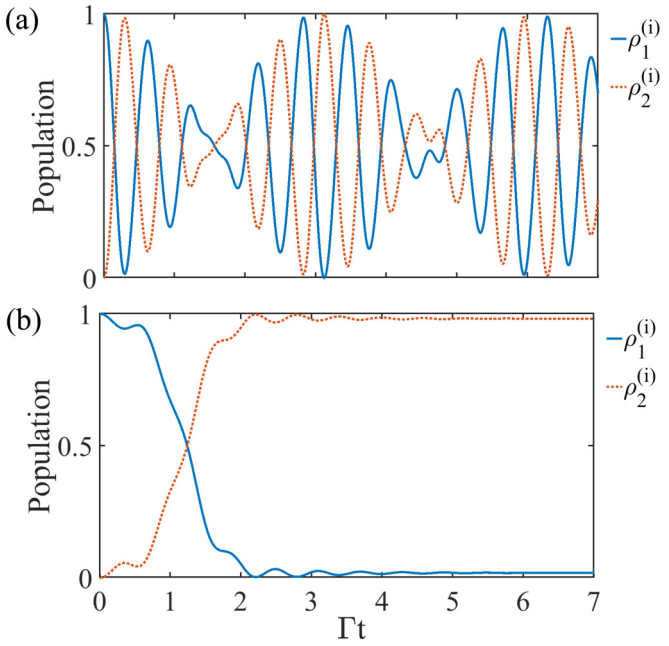

FIG. 4. Populations of H_{eff} for the states $|1\rangle$ (blue solid line) and $|2\rangle$ (orange dotted line) for two interacting particles from the master equation without the quantum jump term. (a) Population in the $\mathcal{PT}$-unbroken phase with the parameters $\Omega = 10\Gamma$ and $V = 2\Gamma$, showing the oscillatory behavior between the two states $|1\rangle$ and $|2\rangle$. (b) Population in the $\mathcal{PT}$-broken phase with $\Omega = 2\Gamma$ and $V = 10\Gamma$, where the population of state $|1\rangle$ decays and then saturates to a fixed value, and the population of state $|2\rangle$ increases and also saturates at a fixed value. We use $\rho_{1,2}^{(i)}$ to designate the population of the particle labeled by the index $i = 1$, 2, 3, and 4 in states $|1\rangle$ and $|2\rangle$. The time axis t has units of $1/\Gamma$.

parameters Ω, Γ, and V are varied; the $\mathcal{PT}$ phase diagrams are shown in Figs. 2(d) and 2(e). These phase diagrams are less rich than the diagrams for the linear chains [see Figs. 2(b) and 2(c)]. We posit that the symmetry of the equilateral triangle and tetrahedral configurations constrains the dynamics and leads to a single $\mathcal{PT}$-symmetry region.

4. *Zigzag configurations*

Next we consider three-particle and four-particle zigzag configurations, parametrized by the angle α as shown in Figs. 1(b) and 1(c); the $\mathcal{PT}$ phase diagrams are presented in Figs. 2(f) and 2(g). As in the previous subsection, the ith and jth atoms interact with dipolar interactions. We define the interaction scale $V_{12} = V$ between nearest neighbors; the interaction strengths between other atom pairs follow from geometrical arguments and are explicitly described in Appendix B. In computing the eigenvalues of $H_{\mathcal{PT}}$, we varied V and α, and we set $\Omega/\Gamma = 10$.

The $\mathcal{PT}$ phase diagrams depend on the angle α as a result of the dependence of interaction strengths V_{ij} on α. We note that in the three-particle configuration when $\alpha = \frac{\pi}{3}$ [black dashed line in Fig. 2(f)] the configuration becomes an equilateral triangle, and we posit that the increased symmetry of the configuration is linked to the crossovers of exceptional lines. In the case of the four-particle configuration, when $\alpha = \frac{\pi}{4}$ in Fig. 1(c), we find the square configuration. The $\mathcal{PT}$ phase

transitions of the linear configurations of $N = 3$ and $N = 4$ particles are retrieved in the limit $\alpha \to \pi$.

B. System with time-dependent parameters

The $\mathcal{PT}$-symmetry phase diagrams can be enriched further by periodically modulating the parameters Ω, V, or Γ with the characteristic frequency ω_F [53]. When the parameters are modulated, the eigenvalues of $\hat{H}_{\mathcal{PT}}$ become time dependent. Then, to study $\mathcal{PT}$ symmetry, instead of calculating whether the eigenvalues of $\hat{H}_{\mathcal{PT}}$ are real, we use the eigenvalues of the time-evolution operator

$$\hat{G}_{\mathcal{PT}}(t) = e^{-i\hat{H}_{\mathcal{PT}}t}. \tag{4}$$

When all the eigenvalues of $\hat{G}_{\mathcal{PT}}(\frac{2\pi}{\omega_F})$ have a unitary modulus, $\mathcal{PT}$ symmetry is preserved, otherwise it is broken.

We adapt the interaction term in $\hat{H}_{\mathcal{PT}}$ [Eq. (3)] for a two-particle system from $V \to V \sin(\omega_F t)$ and calculate the $\mathcal{PT}$-symmetry phase diagrams as the system parameters are varied. In each diagram in Fig. 3, ω_F and either Ω, Γ, or V are varied, while the other two parameters are fixed.

We see that modulation enriches the phase diagrams, because new $\mathcal{PT}$-broken regions appear when the unmodulated model is in the $\mathcal{PT}$-symmetric phase (see Fig. 3). Note that this behavior clearly occurs in Fig. 3(c), where V varies with ω_F, showing a phase transition in the $\mathcal{PT}$-symmetric phase with $\Omega = 10\Gamma$ of the unmodulated model [see Fig. 2(a)].

In Appendix D, we show the $\mathcal{PT}$ phase diagrams for systems of one and two particles when square-wave modulations are applied.

III. PROPOSAL FOR AN EXPERIMENTAL IMPLEMENTATION

Systems of Rydberg atoms and systems of Rydberg ions are well suited for implementing the Hamiltonian in Eq. (2). They can be exquisitely controlled [61,64,65,77] and they exhibit strong dipolar interactions [65]. In a Rydberg system we envisage states $|1\rangle$ and $|2\rangle$ being Rydberg $S_{1/2}$ and $P_{1/2}$ states, with principal quantum numbers around 50. The XY interaction of the form of Eq. (2) can be achieved by coupling the Rydberg $S_{1/2}$ and $P_{1/2}$ states using a near-resonant microwave field; an interaction of this form was used to entangle two trapped ions [73]. Laser light and microwave radiation are used to control systems of Rydberg atoms or ions, including preparing the particles in different states and measuring them in different bases.

By dressing the Rydberg state to other Rydberg or low-lying states, the parameter values can be adjusted across large ranges, which will allow the $\mathcal{PT}$ phase diagrams of Figs. 2 and 3 to be studied. With $^{88}Sr^+$ Rydberg $S_{1/2}$ and $P_{1/2}$ states with principal quantum numbers around 50, the Rydberg states decay due to natural decay and transitions driven by black-body radiation, with a rate of $\Gamma \sim 2\pi \times 10$ kHz. Γ can be tuned by changing the principal quantum number (higher states have lower decay rates), or else Γ can be increased by adding an additional decay channel using a near-resonant laser field; for instance, Γ can easily be increased to $2\pi \times 2$ MHz by using a 306-nm laser field which couples $nS_{1/2} \leftrightarrow 6P_{3/2}$ in the $^{88}Sr^+$ experiment.

The coupling strength Ω between $|1\rangle$ and $|2\rangle$ (that is, the Rydberg $S_{1/2}$ and $P_{1/2}$ states), can be tuned between 0 and $2\pi \times 500$ MHz by changing the intensity of the coupling microwave field.

The interaction strength V can be tuned between 0 and $\approx 2\pi \times 10$ MHz by changing either the principal quantum number of the Rydberg states (lower states interact more weakly), by changing the distance between the ions, or else by changing the detuning of the microwave field from the $S_{1/2} \leftrightarrow P_{1/2}$ resonance [73]. Typical ion separations are around 4 μm.

To modulate the system parameters (as described in Sec. II B), the laser light intensity or the microwave field strength can be modulated, alternatively these fields may be detuned and the detuning may be modulated. Modulation frequencies ω_F between 0 and $\sim 2\pi \times 100$ MHz are achievable.

Ions are routinely trapped in both linear and zigzag configurations [78], while the configurations of atoms in dipole traps can be highly controlled [79]. We simulated systems with interactions $V_{ij} \sim 1/r_{ij}^3$, which has no angular dependence. An interaction of this form can be achieved in a system with dipolar interactions when the particles are in a one-dimensional (two-dimensional) configuration when their dipole moments are perpendicular to the chain (plane) of the particles.

The protocol involves postselecting the results, i.e., removing instances in which the Rydberg states decayed to state $|0\rangle$. This can be achieved using fluorescence detection to distinguish population in $|0\rangle$ from that in $|1\rangle$ and $|2\rangle$. However, since fluorescence detection usually takes more time ($\sim$1 ms) than typical Rydberg-state lifetimes, to reliably achieve postselection the experimentalist may need to transfer population in $|0\rangle$ to an auxilliary state $|0'\rangle$ before conducting postselection. In $^{88}Sr^+$, for example, $|0\rangle$ is the ground state $5S_{1/2}$ and the metastable $4D_{5/2}$ state can serve as an auxiallary state $|0'\rangle$ for hiding population, population can be transferred between these states with high fidelity using a 674-nm laser pulse.

To probe the $H_{\mathcal{PT}}$ dynamics (Fig. 4) the system should be allowed to evolve for different time durations, such that the oscillation period $\sim \frac{2\pi}{\Omega}$ can be resolved. The interesting dynamics has $\Omega \sim \Gamma$, and $\Gamma \sim 2\pi \times 10$ kHz for typical Rydberg systems. Timing resolutions of $\sim$10 ns are routinely achieved in experiments, and so probing the $H_{\mathcal{PT}}$ dynamics should not be problematic from a timing perspective.

IV. CONCLUSIONS

In this work we showed that platforms with few particles with long-range binary interactions are an excellent playground for studying $\mathcal{PT}$-symmetry phase transitions. We find the $\mathcal{PT}$-symmetry phase diagrams become richer as the symmetry of the system is reduced. By modulating the system parameters the phase diagrams can be further enriched. We outline how the $\mathcal{PT}$ symmetry of a system can be determined experimentally, by measuring the evolution of the populations in different states. We expect systems of Rydberg atoms or ions, which exhibit strong dipolar interactions, are particularly suited for experimental studies of the phenomena discussed in this work. We provided realistic predictions for the verification of the dynamical regimes described in the previous sections in Rydberg-ion platforms. In addition, $\mathcal{PT}$-symmetry phase transitions were found by changing the

configurations of the Rydberg atoms. This investigation generalizes previous theoretical and experimental research on effective single-particle models to a many-body environment with direct applications to quantum simulations and quantum information processing.

ACKNOWLEDGMENTS

We gratefully acknowledge stimulating discussions with Y. Pará. T.M. acknowledges CNPq for support through Bolsa de Produtividade em Pesquisa No. 311079/2015-6. This work was supported by the Serrapilheira Institute (Grant No. Serra-1812-27802), by the Knut & Alice Wallenberg Foundation [through the Wallenberg Centre for Quantum Technology (WACQT)], and by the CAPES-STINT project "Strong correlations in Cavity and Ion Quantum Simulators." J.A.S.L. acknowledges Stockholm University for its hospitality. We thank the High Performance Computing Center (NPAD) at UFRN for providing computational resources.

APPENDIX A: SYSTEM POPULATION WITH $\mathcal{PT}$ DYNAMICS FROM THE EXPERIMENTAL ρ_{00} FOR A SINGLE ION

Consider the master equation for the effective Hamiltonian (2) written as follows:

$$\frac{d\hat{\rho}(t)}{dt} = \frac{1}{i}\left[\hat{\mathcal{H}}_{\text{eff}}\hat{\rho}(t) - \hat{\rho}(t)\hat{\mathcal{H}}_{\text{eff}}^{\dagger}\right] = \frac{1}{i}\left[-i\left(\frac{\Gamma_1+\Gamma_2}{2}\right)\hat{\rho}(t) + \hat{\mathcal{H}}_{\mathcal{PT}}\hat{\rho}(t) - \hat{\rho}(t)\hat{\mathcal{H}}_{\mathcal{PT}}^{\dagger}\right], \tag{A1}$$

where we use $\hbar = 1$. For the effective Hamiltonian in Eq. (2), we can choose the density matrix in the form below:

$$\hat{\rho}(t) = \tilde{\rho}(t)\ \exp(-\Gamma' t), \tag{A2}$$

and we find

$$\frac{d\hat{\rho}(t)}{dt} = \exp(-\Gamma' t)\left(\frac{d\tilde{\rho}(t)}{dt} - \Gamma'\tilde{\rho}(t)\right), \tag{A3}$$

where

$$\frac{d\tilde{\rho}(t)}{dt} = \frac{1}{i}(\hat{\mathcal{H}}_{\mathcal{PT}}\tilde{\rho}(t) - \tilde{\rho}(t)\hat{\mathcal{H}}_{\mathcal{PT}}^{\dagger}). \tag{A4}$$

This result can be verified using

$$\tilde{\rho}(t) = \exp(-i\hat{\mathcal{H}}_{\mathcal{PT}})\tilde{\rho}(0)\ \exp(i\hat{\mathcal{H}}_{\mathcal{PT}}^{\dagger}), \tag{A5}$$

with $\tilde{\rho}(0) = \hat{\rho}(0)$. Consider the master equation Eq. (A4) written as follows:

$$\frac{d\tilde{\rho}(t)}{dt} = i\frac{\Omega}{2}(\tilde{\rho}\hat{\sigma}_x - \hat{\sigma}_x\tilde{\rho}) - \frac{\Gamma}{2}(\hat{\sigma}_z\tilde{\rho} + \tilde{\rho}\hat{\sigma}_z). \tag{A6}$$

Using the master equation, Eq. (A6), we determine the following optical Bloch equations of the $\mathcal{PT}$-symmetric non-Hermitian Hamiltonian for $\tilde{\rho}(t)$:

$$\frac{d\tilde{\rho}_{22}(t)}{dt} = i\frac{\Omega}{2}(\tilde{\rho}_{21} - \tilde{\rho}_{12}) - \Gamma\tilde{\rho}_{22}, \tag{A7}$$

$$\frac{d\tilde{\rho}_{11}(t)}{dt} = i\frac{\Omega}{2}(\tilde{\rho}_{12} - \tilde{\rho}_{21}) + \Gamma\tilde{\rho}_{11}, \tag{A8}$$

$$\frac{d\tilde{\rho}_{21}(t)}{dt} = i\frac{\Omega}{2}(\tilde{\rho}_{22} - \tilde{\rho}_{11}), \tag{A9}$$

$$\frac{d\tilde{\rho}_{12}(t)}{dt} = i\frac{\Omega}{2}(\tilde{\rho}_{11} - \tilde{\rho}_{22}). \tag{A10}$$

In this section, we seek to calculate the population of the system with $\mathcal{PT}$ dynamics for the experimentally determined population ρ_{00} of the auxiliary state $|0\rangle$:

$$\rho_{00} = 1 - \exp(-\Gamma' t)\tilde{\rho}_{00} = 1 - \rho_{22} - \rho_{11}. \tag{A11}$$

Here ρ_{22} and ρ_{11} are defined as

$$\rho_{22} = \exp(-\Gamma' t)\tilde{\rho}_{22}, \tag{A12}$$

$$\rho_{11} = \exp(-\Gamma' t)\tilde{\rho}_{11}, \tag{A13}$$

thus,

$$\tilde{\rho}_{00} = \exp(\Gamma' t)(\rho_{22} + \rho_{11}) = \tilde{\rho}_{22} + \tilde{\rho}_{11}. \tag{A14}$$

Then, we find the time evolution of ρ_{00} and $\tilde{\rho}_{00}$ given as follows:

$$\frac{d\rho_{00}(t)}{dt} = \exp(-\Gamma' t)(\Gamma_2\tilde{\rho}_{22} + \Gamma_1\tilde{\rho}_{11}), \tag{A15}$$

$$\frac{d\tilde{\rho}_{00}(t)}{dt} = \Gamma(\tilde{\rho}_{22} - \tilde{\rho}_{11}). \tag{A16}$$

Therefore, accessing both $\tilde{\rho}_{00}$ and $d\tilde{\rho}_{00}/dt$, we find

$$\tilde{\rho}_{22} = \frac{1}{2}\left(\tilde{\rho}_{00} + \frac{1}{\Gamma}\frac{d\tilde{\rho}_{00}}{dt}\right) \tag{A17}$$

and

$$\tilde{\rho}_{11} = \frac{1}{2}\left(\tilde{\rho}_{00} - \frac{1}{\Gamma}\frac{d\tilde{\rho}_{00}}{dt}\right). \tag{A18}$$

Therefore, the quantities in Eq. (A17) and in Eq. (A18) are numerically calculated from the $\mathcal{PT}$-symmetric non-Hermitian Hamiltonian in Eq. (3).

APPENDIX B: INTERACTION STRENGTHS IN THE ZIGZAG CASE

For three particles, the separations between the particles satisfy $r_{12} = r_{23}$ and $r_{13} = 2r_{12}\sin(\alpha/2)$. Thus the interactions strengths are $V_{12} = V_{13} = V$ and $V_{23} = V/[8\sin^3(\alpha/2)]$. For four particles we consider the interactions $V_{12} = V_{23} = V_{34} = \tilde{V}/r^3$, V_{13}, V_{14}, and V_{24} take the following forms:

$$V_{13} = \frac{V}{8\sin^3(\alpha_1/2)}, \tag{B1}$$

$$V_{24} = \frac{V}{8\sin^3(\alpha_2/2)}, \tag{B2}$$

$$V_{14} = \frac{V}{[1 + 4\sin^2(\alpha_1/2) - 4\sin(\alpha_1/2)\cos(\alpha_2+\beta_2)]^{3/2}}, \tag{B3}$$

where α_1, α_2, β_1, and β_2 are the angles between particles. For the forms of the interactions Eqs. (B1), (B2), and (B3), we

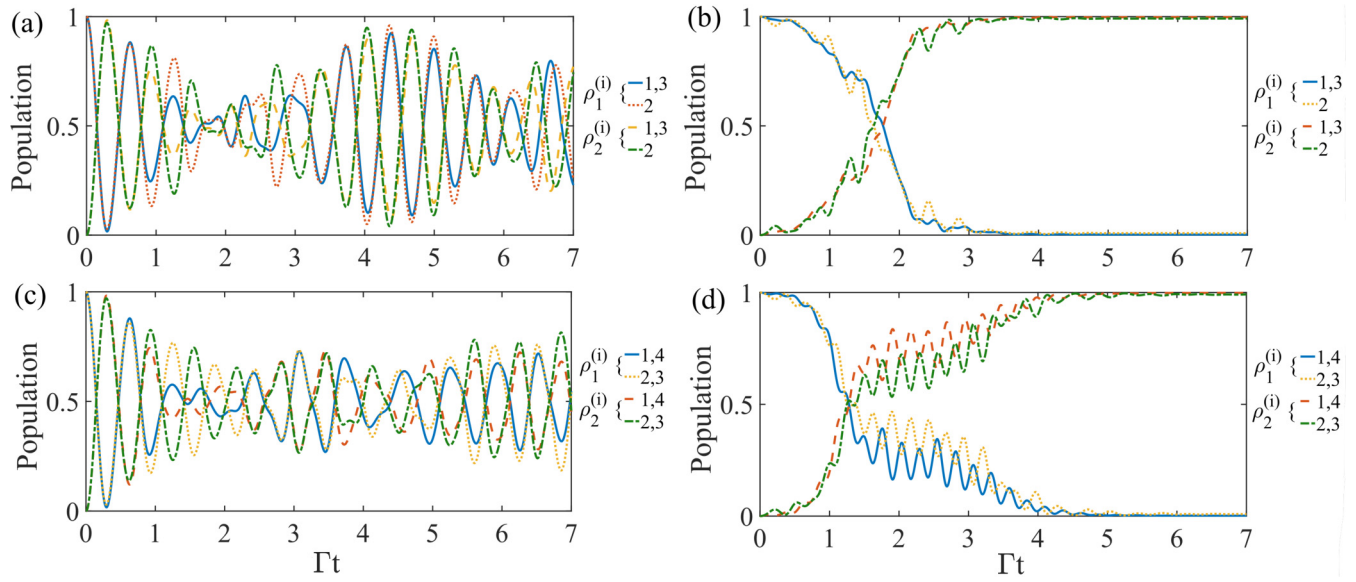

FIG. 5. Populations of Rydberg states $|1\rangle$ and $|2\rangle$ for $N = 3$ and $N = 4$ interacting particles. (a) and (c) $\mathcal{PT}$-symmetric phase ($\Omega = 10\Gamma$ and $V = 2\Gamma$) with oscillatory behavior of Rydberg-state populations. For $N = 3$ particles, the population of particle 1 is equal to that of particle 3 by symmetry in $\rho_1^{(i)}$ and $\rho_2^{(i)}$. In the $N = 4$ case, the population of particle 1 equals the population of particle 4, and similarly for particles 2 and 3. (b) and (d) $\mathcal{PT}$-broken phase ($\Omega = 2\Gamma$ and $V = 10\Gamma$) in which the population of $\rho_1^{(i)}$ decays and the population of $\rho_2^{(i)}$ increases, and both saturate to a fixed value. The time axis t has units of $1/\Gamma$.

take the distances $r_{12} = r_{23} = r_{34} = r$. Therefore, $\alpha_1 = \alpha_2 = \alpha$ and $\beta_1 = \beta_2 = \beta$, and thus, we find $V_{13} = V_{24}$ and V_{14}:

$$V_{14} = \frac{V}{[1 + 4\sin^2(\alpha/2) - 4\sin(\alpha/2)\cos(\alpha+\beta)]^{3/2}}.$$

APPENDIX C: DYNAMICS FOR THREE AND FOUR PARTICLES

In the dynamics for the cases of three and four particles, interactions up to next-next-nearest-neighbors are considered. We chose for the first, second, and third neighbors $V_{\text{first}} = V$, $V_{\text{second}} = V/8$, and $V_{\text{third}} = V/27$, respectively.

In Fig. 5, we show the normalized populations of H_{eff} for $N = 3$ and 4 particles, respectively. In the $\mathcal{PT}$-symmetric region, $\Omega = 10\,\Gamma$ and $V = 2\,\Gamma$ [see Figs. 5(a)–5(c)], we find an oscillatory behavior of states $|1\rangle$ and $|2\rangle$ for the populations of H_{eff}. In the $\mathcal{PT}$-broken region [see Figs. 5(b)–5(d)], $\Omega = 2\,\Gamma$ and $V = 10\,\Gamma$, the population of $\rho_1^{(i)}$ decays and $\rho_1^{(i)}$ is depopulated while the population of $\rho_2^{(i)}$ grows, and both saturate similar to the case of two particles.

APPENDIX D: SQUARE-WAVE MODULATION OF PARAMETERS IN $H_{\mathcal{PT}}$

The Floquet theory applied to $\mathcal{PT}$ symmetry allows the identification of $\mathcal{PT}$-broken phase transitions even in $\mathcal{PT}$-symmetric regions where the eigenvalues of the $\mathcal{PT}$-symmetric Hamiltonian are real [53]. The Hamiltonian of the periodically modulated system is given by

$$H(t) = H(t + T), \tag{D1}$$

where T is the modulation period. In the case of one particle, the periodically modulated $\mathcal{PT}$-symmetric Hamiltonian is given by

$$\hat{H}_{\mathcal{PT}}(t) = \frac{\Omega(t)}{2}\hat{\sigma}_x + i\frac{\Gamma(t)}{2}\hat{\sigma}_z. \tag{D2}$$

For a single particle the propagator reads

$$G_{\mathcal{PT}}(t) = e^{-iH_{\mathcal{PT}}t} = \cos(E_\pm t)\mathbb{I} - i\sin(E_\pm t)\frac{H_{\mathcal{PT}}}{E_\pm}, \tag{D3}$$

where $\mathbb{I}$ is the 2×2 identity matrix and $E_\pm$ are the eigenvalues of $H_{\mathcal{PT}}$. The parameter that indicates the $\mathcal{PT}$ phase transition is given by

$$\Delta e = \frac{|e_1| - |e_2|}{|e_1| + |e_2|}, \tag{D4}$$

where e_1 and e_2 are the eigenvalues of $G_{\mathcal{PT}}$. When $\Delta e = 0$, $\mathcal{PT}$ symmetry is preserved, while when $\Delta e \neq 0$, $\mathcal{PT}$ symmetry is broken.

The coupling Ω is fixed and the dissipation Γ is modulated between Γ_0 and 0 with the Floquet modulation frequency ω_0. Using the following square-wave modulation for $0 \leqslant t < T$, where $T = 2\pi/\omega_0$ is the period of modulation,

$$\Gamma(t) = \begin{cases} \Gamma_0 & 0 \leqslant t < T/2, \\ 0 & T/2 \leqslant t \leqslant T, \end{cases} = \begin{cases} \Gamma_0 & 0 \leqslant t < \pi/\omega_0, \\ 0 & \pi/\omega_0 \leqslant t \leqslant 2\pi/\omega_0. \end{cases} \tag{D5}$$

The time evolution of the system over one period of the driving is the product of the propagators for the static Hamiltonian associated with each step:

$$G_{\mathcal{PT}}(t) = e^{-iH_{\mathcal{PT}}[\Gamma(t)=\Gamma_0]\tau}e^{-iH_{\mathcal{PT}}[\Gamma(t)=0]\tau}, \tag{D6}$$

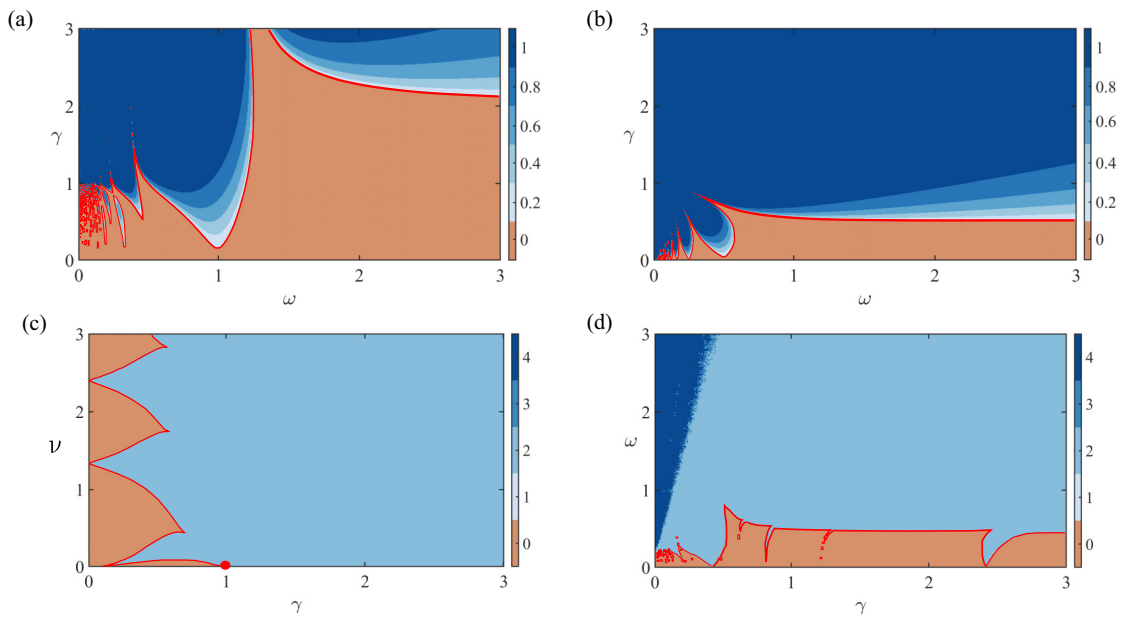

FIG. 6. $\mathcal{PT}$ phase transition diagrams for Hamiltonians of one and two atoms with square-wave modulation. In the case of one atom, the $\mathcal{PT}$ phase transition is represented by Δe. The $\mathcal{PT}$-unbroken phase occurs in $\Delta_e = 0$ and the $\mathcal{PT}$-broken phase consists of the colored region for $\Delta e > 0$. (a) and (b) $\mathcal{PT}$ transition of one atom propagator in Eq. (D7). (c) and (d) $\mathcal{PT}$-phase transition of the propagator of two atoms in Eq. (A13) from eigenvalues with the module different from 1.

where $\tau = T/2$. Therefore, replacing the modulation conditions, we find

$$G_{\mathcal{PT}}\left(\frac{2\pi}{\omega_0}\right) = \exp\left[-i\left(\frac{\hat{\sigma}_x}{2\omega} - i\frac{\gamma}{2\omega}\hat{\sigma}_z\right)\pi\right]\exp\left[-i\frac{\hat{\sigma}_x}{2\omega}\pi\right], \tag{D7}$$

where $\omega \equiv \omega_0/\Omega$, $\gamma \equiv \Gamma_0/\Omega$, and $\nu \equiv V_0/\Omega$. Then, we study the $\mathcal{PT}$ phase diagram of the modulated periodic dissipation Γ and the Rabi frequency Ω. The modulation in Γ is shown in Fig. 6(a), in which the peaks are nonzero values for Δe. When Δe vanishes the system is in the $\mathcal{PT}$-unbroken phase. Figure 6(b) shows the square-wave modulation in Ω similar to Eq. (D4), where again there are $\mathcal{PT}$ transition regions. The colored region describes the $\mathcal{PT}$-broken phase, where $\Delta e > 0$ and the dark blue region describes the $\mathcal{PT}$-unbroken phase at $\Delta e = 0$.

The previous approach describes the time period for one particle. Now, we study the model of two particles in Eq. (3) with periodic modulation. We analyze the phase transition through the relationship of Δe in Eq. (D4). Note that for two particles the $\mathcal{PT}$-symmetric non-Hermitian Hamiltonian has four eigenvalues and Δe has a nonzero value when one of the eigenvalues has a modulus different from 1, indicating the breaking of $\mathcal{PT}$ symmetry. First, we consider the square-wave modulation for the V interaction similar to Eq. (D5), and we keep Ω and Γ fixed. The propagator then reads

$$G_{\mathcal{PT}}(T) = \exp\left[-i\left(\frac{1}{2\omega}\left(\hat{\sigma}_x^2 + \hat{\sigma}_x^1\right) - i\frac{\gamma}{2\omega}\left(\hat{\sigma}_z^2 + \hat{\sigma}_z^1\right) + \frac{\nu}{\omega}\left(\hat{\sigma}_x^1\hat{\sigma}_x^2 + \hat{\sigma}_y^1\hat{\sigma}_y^2\right)\right)\pi\right]\exp\left[-i\left(\frac{1}{2\omega}\left(\hat{\sigma}_x^2 + \hat{\sigma}_x^1\right) - i\frac{\gamma}{2\omega}\left(\hat{\sigma}_z^2 + \hat{\sigma}_z^1\right)\right)\pi\right]. \tag{D8}$$

In Fig. 6(c), we use $\omega = 1$, in this case, we have the regime in which the Rabi frequency Ω is equal to the Floquet frequency ω_0. Note that in the noninteracting regime $\nu = 0$, the $\mathcal{PT}$ symmetry is preserved for values of $\gamma < 1$, and for values of $\gamma > 1$ the $\mathcal{PT}$ symmetry is broken, presenting an exceptional point in $\gamma = 1$ described by the red dot, which in this static case also presents the same exceptional point. The exceptional line is given by the red line that separates the $\mathcal{PT}$-symmetric and $\mathcal{PT}$-broken regions.

We take the modulation for the Γ dissipation, whose propagator is given through square-wave modulation in the form of Eq. (D5). Setting $\nu = \Gamma$, we find the $\mathcal{PT}$ phase transition diagram, which also has symmetry-breaking phases [see Fig. 6(d)].

[1] N. Moiseyev, *Non-Hermitian Quantum Mechanics* (Cambridge University, Cambridge, England, 2011).
[2] I. Rotter, J. Phys. A: Math. Theor. **42**, 153001 (2009).
[3] A. Eckardt and E. Anisimovas, New J. Phys. **17**, 093039 (2015).
[4] C. M. Bender and S. Boettcher, Phys. Rev. Lett. **80**, 5243 (1998).

[5] C. M. Bender and D. W. Darg, J. Math. Phys. **48**, 042703 (2007).
[6] W. D. Heiss, J. Phys. A: Math. Theor. **45**, 444016 (2012).
[7] B.-B. Wei and L. Jin, Sci. Rep. **7**, 7165 (2017).
[8] K. Moors, A. A. Zyuzin, A. Y. Zyuzin, R. P. Tiwari, and T. L. Schmidt, Phys. Rev. B **99**, 041116(R) (2019).
[9] Z. Yang and J. Hu, Phys. Rev. B **99**, 081102(R) (2019).
[10] Z. Zhang, Z. Yang, and J. Hu, Phys. Rev. B **102**, 045412 (2020).
[11] C. E. Rüter, K. G. Makris, R. El-Ganainy, D. N. Christodoulides, M. Segev, and D. Kip, Nat. Phys. **6**, 192 (2010).
[12] A. A. Zyablovsky, A. P. Vinogradov, A. A. Pukhov, A. V. Dorofeenko, and A. A. Lisyansky, Phys.-Usp. **57**, 1063 (2014).
[13] P. Lodahl, S. Mahmoodian, S. Stobbe, A. Rauschenbeutel, P. Schneeweiss, J. Volz, H. Pichler, and P. Zoller, Nature (London) **541**, 473 (2017).
[14] R. El-Ganainy, K. G. Makris, M. Khajavikhan, Z. H. Musslimani, S. Rotter, and D. N. Christodoulides, Nat. Phys. **14**, 11 (2018).
[15] S. Longhi, Opt. Lett. **43**, 2929 (2018); **43**, 5371 (2018); **43**, 4025 (2018); **44**, 5804 (2019); **45**, 1591 (2020).
[16] C. M. Bender, P. E. Dorey, C. Dunning, A. Fring, D. W. Hook, H. F. Jones, S. Kuzhel, G. Lévai, and R. Tateo, *PT Symmetry* (World Scientific, London, 2019).
[17] L. Feng, R. El-Ganainy, and L. Ge, Nat. Photonics **11**, 752 (2017).
[18] H. Zhao and L. Feng, Natl. Sci. Rev. **5**, 183 (2018).
[19] C. K. Özdemir, S. Rotter, F. Nori, and L. Yang, Nat. Mater. **18**, 783 (2019).
[20] F. Klauck, L. Teuber, M. Ornigotti, M. Heinrich, S. Scheel, and A. Szameit, Nat. Photonics **13**, 883 (2019).
[21] S.-M. Fei, Czech. J. Phys. **53**, 1572 (2003).
[22] C. Korff and R. Weston, J. Phys. A: Math. Theor. **40**, 8845 (2007).
[23] O. A. Castro-Alvaredo and A. Fring, J. Phys. A: Math. Theor. **42**, 465211 (2009).
[24] T. Deguchi and P. K. Ghosh, J. Phys. A: Math. Theor. **42**, 475208 (2009).
[25] C. M. Bender, J. Phys.: Conf. Ser. **631**, 012002 (2015).
[26] Y. Ashida, S. Furukawa, and M. Ueda, Phys. Rev. A **94**, 053615 (2016); Nat. Commun. **8**, 15791 (2017); Y. Ashida, K. Saito, and M. Ueda, Phys. Rev. Lett. **121**, 170402 (2018); Y. Ashida, Z. Gong, and M. Ueda, Adv. Phys. **69**, 249 (2020).
[27] K. Kawabata, Y. Ashida, and M. Ueda, Phys. Rev. Lett. **119**, 190401 (2017).
[28] J. A. S. Lourenço, R. L. Eneias, and R. G. Pereira, Phys. Rev. B **98**, 085126 (2018).
[29] M. Nakagawa, N. Kawakami, and M. Ueda, Phys. Rev. Lett. **121**, 203001 (2018).
[30] R. Hamazaki, K. Kawabata, and M. Ueda, Phys. Rev. Lett. **123**, 090603 (2019).
[31] K. Yamamoto, M. Nakagawa, K. Adachi, K. Takasan, M. Ueda, and N. Kawakami, Phys. Rev. Lett. **123**, 123601 (2019).
[32] L. Xiao, K. Wang, X. Zhan, Z. Bian, K. Kawabata, M. Ueda, W. Yi, and P. Xue, Phys. Rev. Lett. **123**, 230401 (2019).
[33] N. Matsumoto, K. Kawabata, Y. Ashida, S. Furukawa, and M. Ueda, Phys. Rev. Lett. **125**, 260601 (2020).
[34] E. Lee, H. Lee, and B.-J. Yang, Phys. Rev. B **101**, 121109(R) (2020).
[35] H. Shackleton and M. S. Scheurer, Phys. Rev. Research **2**, 033022 (2020).
[36] S. Weidemann, M. Kremer, S. Longhi, and A. Szameit, arXiv:2007.00294.
[37] Y. Takasu, T. Yagami, Y. Ashida, R. Hamazaki, Y. Kuno, and Y. Takahashi, Prog. Theor. Exp. Phys. **2020**, 12A110 (2020).
[38] J. Huber, P. Kirton, S. Rotter, and P. Rabl, SciPost Phys. **9**, 052 (2020).
[39] K. Yamamoto, Y. Ashida, and N. Kawakami, Phys. Rev. Research **2**, 043343 (2020).
[40] D. P. Pires and T. Macrì, Phys. Rev. B **104**, 155141 (2021).
[41] C. Yuce and Z. Oztas, Sci. Rep. **8**, 17416 (2018); C. Yuce, Phys. Rev. A **97**, 042118 (2018).
[42] K. Wang, X. Qiu, L. Xiao, X. Zhan, Z. Bian, B. C. Sanders, W. Yi, and P. Xue, Nat. Commun. **10**, 2293 (2019).
[43] S. Longhi, Phys. Rev. Lett. **122**, 237601 (2019).
[44] K. Kawabata, K. Shiozaki, M. Ueda, and M. Sato, Phys. Rev. X **9**, 041015 (2019).
[45] M. Kawasaki, K. Mochizuki, N. Kawakami, and H. Obuse, Prog. Theor. Exp. Phys. **2020**, 12A105 (2020).
[46] P.-Y. Chang, J.-S. You, X. Wen, and S. Ryu, Phys. Rev. Research **2**, 033069 (2020).
[47] Z. Xu, R. Zhang, S. Chen, L. Fu, and Y. Zhang, Phys. Rev. A **101**, 013635 (2020).
[48] E. N. Blose, Phys. Rev. B **102**, 104303 (2020).
[49] C.-X. Guo, X.-R. Wang, and S.-P. Kou, Europhys. Lett. **131**, 27002 (2020).
[50] V. Mittal, A. Raj, S. Dey, and S. K. Goyal, Sci. Rep. **11**, 10262 (2021).
[51] S. Xia, D. Kaltsas, D. Song, I. Komis, J. Xu, A. Szameit, H. Buljan, K. G. Makris, and Z. Chen, Science **372**, 72 (2021).
[52] Y. Pará, G. Palumbo, and T. Macrì, Phys. Rev. B **103**, 155417 (2021).
[53] J. Li, A. K. Harter, J. Liu, L. de Melo, Y. N. Joglekar, and L. Luo, Nat. Commun. **10**, 855 (2019).
[54] A. K. Harter and N. Hatano, arXiv:2006.16890.
[55] A. K. Harter and Y. N. Joglekar, Prog. Theor. Exp. Phys. **2020**, 12A106 (2021).
[56] W.-C. Wang, Y.-L. Zhou, H.-L. Zhang, J. Zhang, M.-C. Zhang, Y. Xie, C.-W. Wu, T. Chen, B.-Q. Ou, W. Wu, H. Jing, and P.-X. Chen, Phys. Rev. A **103**, L020201 (2021).
[57] L. Ding, K. Shi, Q. Zhang, D. Shen, X. Zhang, and W. Zhang, Phys. Rev. Lett. **126**, 083604 (2021).
[58] N. Defenu, T. Donner, T. Macrì, G. Pagano, S. Ruffo, and A. Trombettoni, arXiv:2109.01063.
[59] L. Béguin, A. Vernier, R. Chicireanu, T. Lahaye, and A. Browaeys, Phys. Rev. Lett. **110**, 263201 (2013).
[60] T. Macrì and T. Pohl, Phys. Rev. A **89**, 011402(R) (2014).
[61] D. Barredo, H. Labuhn, S. Ravets, T. Lahaye, A. Browaeys, and C. S. Adams, Phys. Rev. Lett. **114**, 113002 (2015).
[62] J. Zeiher, P. Schauß, S. Hild, T. Macrì, I. Bloch, and C. Gross, Phys. Rev. X **5**, 031015 (2015).
[63] H. Labuhn, D. Barredo, S. Ravets, S. de Léséleuc, T. Macrì, T. Lahaye, and A. Browaeys, Nature (London) **534**, 667 (2016).
[64] S. Ravets, J. Hoffman, F. Fatemi, S. Rolston, L. Orozco, D. Barredo, H. Labuhn, T. Lahaye, and A. Browaeys, in *Frontiers in Optics 2016* (Optica Publishing Group, New York, 2016), paper LTu1E.4.

[65] A. Browaeys, D. Barredo, and T. Lahaye, J. Phys. B: At. Mol. Opt. Phys. **49**, 152001 (2016); A. Browaeys, Many-body physics with arrays of Rydberg atoms, in *Proceedings of Séminaire NCCR, QSIT–Quantum Science and Technology, Physics Department, ETH Zürich, Switzerland, November 2, 2017* (University of Basel, 2017); A. Browaeys and T. Lahaye, Nat. Phys. **16**, 132 (2020).

[66] P. Scholl, M. Schuler, H. J. Williams, A. A. Eberharter, D. Barredo, K.-N. Schymik, V. Lienhard, L.-P. Henry, T. C. Lang, T. Lahaye, A. M. Läuchli, and A. Browaeys, Nature (London) **595**, 233 (2021).

[67] S. de Léséleuc, V. Lienhard, P. Scholl, D. Barredo, S. Weber, N. Lang, H. P. Büchler, T. Lahaye, and A. Browaeys, Science **365**, 775 (2019).

[68] L. Henriet, L. Beguin, A. Signoles, T. Lahaye, A. Browaeys, G.-O. Reymond, and C. Jurczak, Quantum **4**, 327 (2020).

[69] S. Hermes, T. J. G. Apollaro, S. Paganelli, and T. Macrì, Phys. Rev. A **101**, 053607 (2020).

[70] T. Macrì, L. Lepori, G. Pagano, M. Lewenstein, and L. Barbiero, Phys. Rev. B **104**, 214309 (2021).

[71] Z. Z. Yan, J. W. Park, Y. Ni, H. Loh, S. Will, T. Karman, and M. Zwierlein, Phys. Rev. Lett. **125**, 063401 (2020).

[72] Y. Lin, D. R. Leibrandt, D. Leibfried, and C.-w. Chou, Nature (London) **581**, 273 (2020).

[73] C. Zhang, F. Pokorny, W. Li, G. Higgins, A. Pöschl, I. Lesanovsky, and M. Hennrich, Nature (London) **580**, 345 (2020).

[74] F. Minganti, A. Miranowicz, R. W. Chhajlany, and F. Nori, Phys. Rev. A **100**, 062131 (2019).

[75] M. Naghiloo, M. Abbasi, Y. N. Joglekar, and K. W. Murch, Nat. Phys. **15**, 1232 (2019).

[76] W. Chen, M. Abbasi, Y. N. Joglekar, and K. W. Murch, Phys. Rev. Lett. **127**, 140504 (2021).

[77] S. Ebadi, T. T. Wang, H. Levine, A. Keesling, G. Semeghini, A. Omran, D. Bluvstein, R. Samajdar, H. Pichler, W. W. Ho, S. Choi, S. Sachdev, M. Greiner, V. Vuletić, and M. D. Lukin, Nature (London) **595**, 227 (2021).

[78] M. G. Raizen, J. M. Gilligan, J. C. Bergquist, W. M. Itano, and D. J. Wineland, Phys. Rev. A **45**, 6493 (1992).

[79] D. Barredo, V. Lienhard, S. de Léséleuc, T. Lahaye, and A. Browaeys, Nature (London) **561**, 79 (2018).